Antiresonant Fabry-Pérot cavity with ultralow finesse

Tiantian Shi, Jianxiang Miao, Jia Zhang, and Jingbiao Chen*

State Key Laboratory of Advanced Optical Communication Systems and Networks, Institute of Quantum Electronics, School of Electronics, Peking University, Beijing 100871, China

(Received 20 September 2022; accepted 6 February 2023; published 22 February 2023)

The exact expressions of finesse and full width at half maximum (FWHM) of the Airy distribution of a Fabry-Pérot (FP) resonator are derived, which solves the breakdown problem at ultralow reflectivity in traditional formulas. We demonstrate that, when the cavity-mirror reflectivity $R \to 0$, the FWHM approaches half of the free spectral range rather than infinity; moreover, the cavity finesse $\mathcal{F}$ approaches 2 rather than zero. These expressions are useful for the development of bad-cavity lasers, such as the four-level active optical clock based on the strong atomic transition of cesium. Also, the exact expressions of the FWHM and finesse of the reflection distribution composed of reflected mode profiles are derived, which separately intersect with that of the Airy one at $R = 0$. In addition, the characteristics of an antiresonant cavity, the frequency of which is exactly at the center of two adjacent resonant cavity modes, are analyzed. It is demonstrated that at the resonant and antiresonant frequencies the enhancement and inhibition of intracavity light intensity caused by the FP cavity are symmetrical in the logarithmic view. Furthermore, we provide a universal expression of the cavity-enhancement factor rather than the classical representation of "$2\mathcal{F}/\pi$," which is inadequate for the high-loss cavity because the cavity-enhancement factor should naturally reach 1 when $R \to 0$. Finally, we extend the application of the antiresonant cavity to an inhibited laser, the frequency of which has a stronger suppression effect on the cavity-length thermal noise than the traditional resonant laser.

DOI: 10.1103/PhysRevA.107.023517

I. INTRODUCTION

Laser stabilization, which is used to generate a highly coherent and stable light source, is critical for achieving optical atomic clocks with high quality factor. Utilizing the Pound-Drever-Hall technique [1,2], the Fabry-Pérot (FP) cavity with ultrahigh reflectivity is optimal to stabilize the laser frequency. Owing to the ultranarrow resonant bandwidth, the laser frequency is locked to a small resonant range, which generates a laser with a narrowest linewidth of sub-10 mHz [3]. Such frequency stabilization utilizes the cavity-enhancement effect of a resonant FP cavity.

Except for the application of frequency stabilization, the cavity-enhancement effect of a resonant cavity is significant for atom-cavity coupling. The interaction between the intracavity photons and the atom is greatly enhanced when the atom is coupled to a resonant cavity, which is famous for the Purcell effect first proposed by Purcell in 1946 [4]. Because the large Purcell factor requires a high-Q resonator with a small mode volume, it was not until about 40 years later that the Purcell effect was experimentally proven in microwave [5] and optical [6,7] resonant cavities.

Moreover, the feasibility of balancing the damping rate of the field in a cavity and the spontaneous emission rate with a high-Q resonant cavity has wide application in both the weak- and strong-coupling limits. In a weakly coupled cavity, the cavity-enhancement effect is widely used for semiconductor microcavity structures to provide the wafers for vertical-cavity surface-emitting lasers. In addition, the high-reflectivity resonant cavities are also commonly used to generate low-threshold lasers [8–10]. Such a design is a key ingredient for laser oscillation, and improves the directionality of radiation. In the strong-coupling limit, the cavity enhancement effect is significant for cavity quantum electrodynamics (QED). The interaction between the intracavity photons and the atom is reversible, which is critical in the development of single-photon phase gates for use in quantum computers [11].

Based on the above-mentioned advantages, the characteristics of a resonant cavity with high reflectivity are fully analyzed. Therefore, the basic expressions for the characteristics of an FP cavity, such as the cavity finesse and cavity-mode linewidth of the Airy distribution, as well as the cavity-enhancement effect, are limited to the resonant high-Q-factor condition, resulting in the analysis under low-reflectivity conditions being missed. However, high-reflectivity FP cavities tend to introduce some complexity along with their great superiority. For instance, to optimize the fractional stability of the optical length of the cavity, FP resonators are built based on well-isolated cryogenically cooled single-crystal silicon [3,12], and with ultrahigh dielectric coatings, which will increase the production costs and technical complexity. In addition, the higher the cavity reflectivity is, the sharper the cavity profile becomes, and the cavity-mode frequency is more susceptible to the thermal noise of the cavity length.

Alternatively, by using a cavity with ultralow finesse, the above problems will be solved. A typical application is an active optical clock (AOC) [13–22] based on strong atomic transition of cesium [20,23]. Working in the bad-cavity limit [13,15,16,18–20,22], where the atomic decay rate Γ_{gain} is

*jbchen@pku.edu.cn

much smaller than the cavity dissipation rate Γ_c, only weak cavity-induced feedback occurs on the atomic dipole, resulting in the collective atomic dipole being highly coherent, and the phase information of an AOC laser is primarily stored in the atomic gain medium. Therefore, compared with the good-cavity laser using an ultrahigh-finesse optical cavity as a reference, the sensitivity of an AOC laser to cavity fluctuations is greatly reduced, as characterized by the suppressed cavity-pulling effect. The analysis of a low-reflectivity cavity is significant for the research of AOC lasers. It is urgent to find universal expressions applicable for any reflectivity. Moreover, the theoretical analysis of a cavity operating at any frequency, let alone at the antiresonant region—namely the cavity frequency being at the center of two adjacent resonant frequencies—is missing.

To solve these problems, in this paper we provide the exact expressions of finesse and full width at half maximum (FWHM) of the Airy distribution of a FP resonator both at the resonant and antiresonant frequencies, and we successfully solve the breakdown problem [24] at ultralow reflectivity in traditional formulas. We demonstrate that, when the cavity-mirror reflectivity $R \to 0$, the FWHM approaches half of the free spectral range (FSR) rather than infinity, and the finesse $\mathcal{F}$ approaches 2 rather than zero. In addition, a universal expression of the cavity-enhancement factor rather than the classical representation of $2\mathcal{F}/\pi$ is given. Because the cavity-enhancement factor should naturally reach 1 when $R \to 0$, the traditional expression is inapplicable for the high-loss cavity.

Moreover, we extend the application of an antiresonant cavity with ultralow finesse to realize an inhibited laser [25], the frequency of which has a stronger suppression effect on the cavity-length thermal noise than a traditional resonant laser. Working in the antiresonant cavity region, the cavity-loss term in the laser rate equation of an inhibited laser is rewritten. We provide the expression of loss term and prove it in the photon picture. This indicates that, as $R \to 0$, the loss factor approaches 1 in both resonant and antiresonant regimes. Regarding $R \to 1$, the loss factor at resonance is $2\mathcal{F}/\pi$ times that at the antiresonance case. Therefore, it is easier to realize laser oscillation in the antiresonant region with a low-finesse resonator. In addition, we analyze the cavity-pulling coefficient of a traditional resonant laser and inhibited laser under arbitrary reflectivity. The influence of cavity-length noise on the frequency of an inhibited laser can be further suppressed by a factor of $(\frac{1+R}{1-R})^2$ times.

The application of an inhibited laser is expected to connect multiple research fields, such as atomic optical clocks, laser physics, quantum metrology, and cavity QED, and it will greatly facilitate precision measurements for fundamental science. Our findings represent a vivid example of intuitively applying an antiresonant inhibited laser with the advantage of suppressing the cavity-pulling effect, which will broaden the horizon of quantum metrology and laser physics.

The rest of this paper is organized as follows. In Sec. II, the characteristics of a FP cavity are introduced. According to the Airy function and power reflection factor, the exact expressions of cavity finesse and the FWHM of Airy and reflection distributions are obtained. Moreover, the FWHM and finesse of the antiresonant cavity are given, which intersect with the results of the resonant condition at $R = 0$ respectively. In addition, the cavity-enhancement factor with the change of cavity frequency at different cavity-mirror reflectivities is analyzed. In particular, the cavity-enhancement effect at the resonant regime and the cavity-inhibition effect at the antiresonant regime are symmetrical in the logarithmic view. Section III presents the application of the antiresonant FP cavity, which is used for the realization of the inhibited laser with the advantage of enhanced cavity-pulling effect. Conclusions are drawn in Sec. IV.

II. GENERAL EXPRESSIONS FOR FP-CAVITY CHARACTERISTICS

An ultrastable optical cavity, which is aimed at generating a highly phase-coherent and frequency-stable laser source, has become a powerful tool for laser frequency stabilization [1,26]. Before studying the interaction between atoms and a cavity, it is necessary to thoroughly investigate the basic properties of an optical cavity. In this section, the exact expressions of finesse and the FWHM of an optical cavity under any cavity-mirror reflectivity are derived, which are slightly different from the results under the condition of high reflectivity expressed in most classical optical texts [27,28]. Moreover, the general expression of the cavity-enhancement factor at any reflectivity is demonstrated. We also prove that the intracavity light intensities enhanced by the resonant cavity and inhibited by the antiresonant cavity are symmetrical at the condition of the same cavity-mirror reflectivity.

A. Airy function and power reflection factor

Here, we consider a typical model of an optical cavity [28], which consists of a simple two-mirror FP interferometer separated by a distance L, as depicted in Fig. 1(a). The complex amplitude reflection and transmission coefficients of plane mirror M_1 and plane-parallel mirror M_2 are r_1, t_1 and r_2, t_2, respectively. $R_1 = {r_1}^2$, $R_2 = {r_2}^2$ and $T_1 = {t_1}^2$, $T_2 = {t_2}^2$ are the reflectivity and transmittance of M_1 and M_2, respectively. Considering that the complex amplitude of the electromagnetic wave incident at M_1 is E_0, E_T and E_R are the respective amplitudes of the waves that are transmitted and reflected by the FP cavity.

The ratio of light power transmitting through the cavity to that of the incident radiation, i.e., the so-called Airy function [28], is expressed as

$$T(\omega) = \frac{E_T E_T^*}{{E_0}^2} = \frac{{t_1}^2 {t_2}^2}{1 + {r_1}^2 {r_2}^2 - 2r_1 r_2 \cos(\omega 2L/c)}, \quad (1)$$

where $\Delta\phi = \omega 2L/c$ represents the phase shift, ω is the angular frequency of the incident radiation, and c is the speed of light. Accordingly, the power reflected by the resonator is given by

$$R(\omega) = \frac{E_R E_R^*}{{E_0}^2} = \frac{2r_1 r_2[1 - \cos(\omega 2L/c)]}{1 + {r_1}^2 {r_2}^2 - 2r_1 r_2 \cos(\omega 2L/c)}. \quad (2)$$

According to Eqs. (1) and (2), the transmittance and reflection both depend on the phase shift $\Delta\phi$. The transmission $T(\omega)$ and reflection $R(\omega)$ factors are sketched in Fig. 2, which satisfies the condition of $T(\omega)+R(\omega) = 1$. It should be noted that the Airy function is also applicable to the condition that

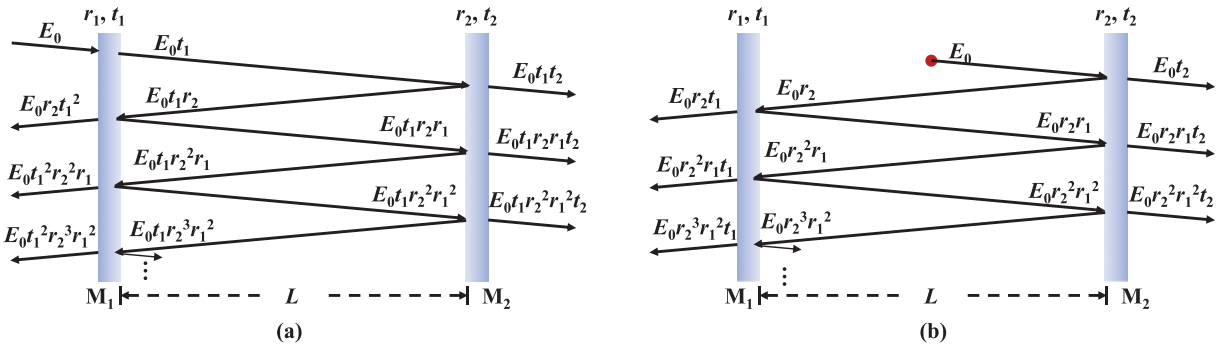

FIG. 1. Amplitudes of waves transmitted and reflected by the FP cavity. (a) Initial wave incident on one of the mirrors of the FP cavity. (b) Emitter locating at the center of the FP cavity and radiating the initial electromagnetic wave.

the initial emitter radiates at the location of $L/2$, as shown in Fig. 1(b).

Obviously, the transmission of the FP cavity at the antiresonant region, namely that the cavity-mode frequency is exactly at the center of two adjacent cavity modes, increases gradually as the cavity reflectivity increases. Moreover, the FWHM at the resonant regime becomes larger with increasing reflectivity. The result of power reflection is opposite that of power transmittance.

B. Exact expressions of cavity finesse and FWHM

For an empty FP cavity, the maximum and minimum transmittances according to Eq. (1) are

$$T_{\max} = \frac{{t_1}^2{t_2}^2}{1 + {r_1}^2{r_2}^2 - 2r_1r_2} \tag{3}$$

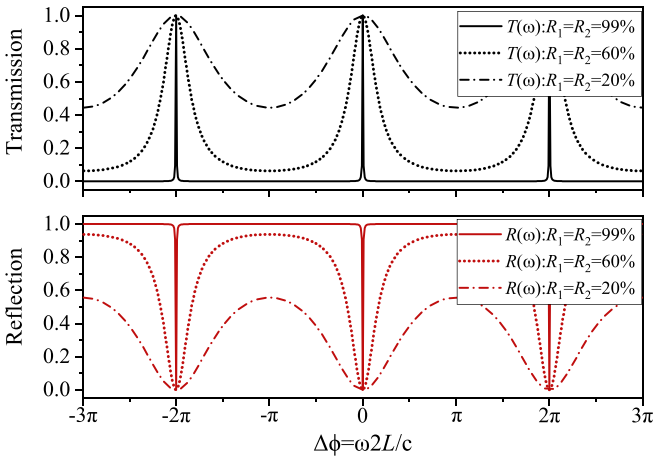

FIG. 2. Ratio of light intensity passed through (reflected from) the FP cavity to that of the incident radiation vs phase shift, resulting in a periodic set of transmitted (reflected) peaks. Transmission reaches maximum when light frequency coincides with cavity resonance, and reaches minimum when light frequency is exactly between two cavity resonances. Power reflection is opposite that of transmittance reflection. Upper and lower subfigures represent transmission and reflection, respectively, and they share a horizontal coordinate. Solid, dotted, and dashed-dotted lines correspond to cavity-mirror reflectivities of $R_1 = R_2 = 99$, 60, and 20%, respectively. Relationships between cavity-mode linewidth $\Delta\nu_{\rm r}$ and $\Delta\nu_{\rm antires}$ are given by $\Delta\nu_{\rm antires} = R_{\rm FS} - \Delta\nu_{\rm r}$.

and

$$T_{\min} = \frac{{t_1}^2{t_2}^2}{1 + {r_1}^2{r_2}^2 + 2r_1r_2}, \tag{4}$$

which correspond to the cases that the cavity frequency is in the vicinity of the qth resonance frequency ω_q and that the cavity frequency is located exactly between two adjacent cavity resonances, respectively. Because the minimum transmittance $T_{\min}$ is negligible under high-reflectivity conditions, the FWHM is usually expressed as the frequency difference at half of the maximum transmittance of one of the transmission spectra [27,28]. However, as the reflectivity of the cavity mirror decreases, $T_{\min}$ increases so that the value of $T_{\min}$ cannot be omitted for the calculation of the FWHM. To obtain a universal expression, we express the FWHM as the frequency difference at which the transmittance equals half of the sum of $T_{\max}$ and $T_{\min}$:

$$T(\omega) = \tfrac{1}{2}(T_{\max} + T_{\min}). \tag{5}$$

From Eqs. (1) and (5), we can derive the values of ω. Then, the FWHM of one of the periodic transmission spectra (cavity bandwidth) without approximation of a resonant cavity is given by

$$\Delta\nu_{\rm r} = \frac{\Delta\omega_{\rm r}}{2\pi} = \frac{R_{\rm FS}}{\pi}\arccos\left(\frac{2r_1r_2}{1 + {r_1}^2{r_2}^2}\right), \tag{6}$$

where the free spectral range $R_{\rm FS} = c/2L$. Accordingly, the finesse of the FP interferometer is

$$\mathcal{F}_{\rm r} = \frac{R_{\rm FS}}{\Delta\nu_{\rm r}} = \frac{\pi}{\arccos\left(\frac{2r_1r_2}{1+{r_1}^2{r_2}^2}\right)}. \tag{7}$$

It should be pointed out that when the mirrors' reflectivity is close to 1, Eqs. (6) and (7) are reduced to the traditional expressions [27,28], as follows:

$$\Delta\nu_{\rm r}' = R_{\rm FS}\frac{1 - r_1r_2}{\pi\sqrt{r_1r_2}} \tag{8}$$

and

$$\mathcal{F}_{\rm r}' = \frac{\pi\sqrt{r_1r_2}}{1 - r_1r_2}. \tag{9}$$

However, if the reflectivities of the cavity mirrors are extremely low, or even close to zero, Eq. (7) can be expressed

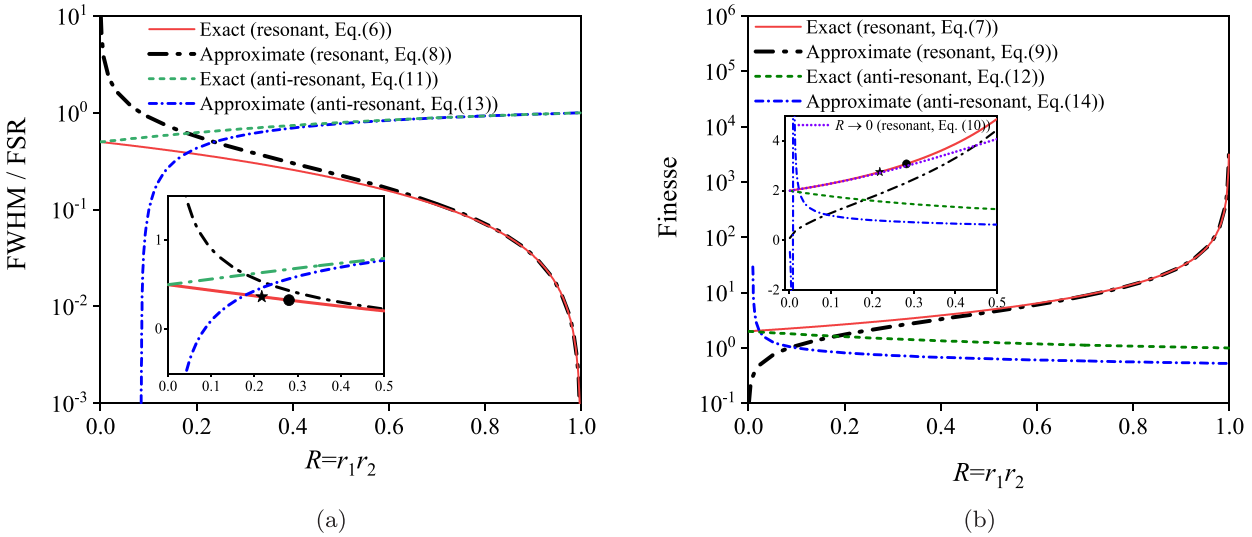

FIG. 3. (a) Ratio of the FWHM to the FSR and (b) finesse with the change of cavity-mirror reflectivity $R = r_1 r_2$ when the FP cavity is resonant and antiresonant with incident light, respectively. The main plots are presented in logarithmic scales, and the insets are in linear scales. The solid red line and the dashed green line represent exact solutions, while the dashed-dotted black line and the short-dashed-dotted blue line depict results with the high-reflectivity approximation. This illustrates that whether the cavity is resonant or antiresonant, the exact and approximate solutions tend to coincide when R is larger than 0.7 but separate below 0.7. These results are shown clearly in the insets with R in the range 0–0.5. The insets also confirm that the exact expressions are credible, because there is an intersection of the resonant and antiresonant results at $R = 0$, while there are break points in the approximate results. The purple dotted line in the inset represents Eq. (10). Since Eq. (10) is the approximate result of the cavity finesse when the reflectivity is extremely low, with increasing reflectivity, the results represented by Eqs. (10) and (9) gradually separate. Black stars and black circles represent experimental values from our previous work [20,25].

through a Taylor formula as

$$\mathcal{F}_{\mathrm{r}}'' = \frac{\pi}{\frac{\pi}{2} - \frac{2r_1 r_2}{1+r_1^2 r_2^2}} = 2 + \frac{8r_1 r_2}{\pi\left(1 + r_1^2 r_2^2\right) - 4r_1 r_2}. \tag{10}$$

It is clear that, when R approaches zero, the cavity finesse reaches the minimum of 2, which is different from the result obtained from Eq. (9).

Generally, for laser oscillation, the cavity-mode frequency is tuned to the exact resonant frequency for generating a highly coherent laser source. The counterintuitive antiresonant cavity, the cavity frequency of which is exactly between two adjacent cavity resonances, is rarely considered. However, the lasing output from an antiresonance cavity is achievable, and has many unique properties. To distinguish the antiresonant cavity from the traditional resonant one, the cavity bandwidth $\Delta\nu_{\mathrm{antires}}$ and finesse $\mathcal{F}_{\mathrm{antires}}$ of the antiresonant cavity are described by Eqs. (11) and (12), respectively, as

$$\Delta\nu_{\mathrm{antires}} = R_{\mathrm{FS}} - \Delta\nu_{\mathrm{r}} = R_{\mathrm{FS}}\left[1 - \frac{1}{\pi}\arccos\left(\frac{2r_1 r_2}{1 + r_1^2 r_2^2}\right)\right] \tag{11}$$

and

$$\mathcal{F}_{\mathrm{antires}} = \frac{R_{\mathrm{FS}}}{\Delta\nu_{\mathrm{antires}}} = \frac{1}{1 - \frac{1}{\pi}\arccos\left(\frac{2r_1 r_2}{1+r_1^2 r_2^2}\right)}. \tag{12}$$

Similarly, Eqs. (11) and (12) are reduced to Eqs. (13) and (14) under a high-reflectivity approximation, as

$$\Delta\nu_{\mathrm{antires}}' = R_{\mathrm{FS}}\left(1 - \frac{1 - r_1 r_2}{\pi\sqrt{r_1 r_2}}\right) \tag{13}$$

and

$$\mathcal{F}_{\mathrm{antires}}' = \frac{1}{1 - \frac{1-r_1 r_2}{\pi\sqrt{r_1 r_2}}}, \tag{14}$$

respectively. When the reflectivity is extremely low, Eq. (12) can be written as

$$\mathcal{F}_{\mathrm{antires}}'' = \frac{1}{1 - \frac{1}{\pi}\left(\frac{\pi}{2} - \frac{2r_1 r_2}{1+r_1^2 r_2^2}\right)} = 2 - \frac{8r_1 r_2}{\pi\left(1 + r_1^2 r_2^2\right) + 4r_1 r_2}, \tag{15}$$

which reaches a maximum of 2 and coincides with the value in the case of the resonance when $R = 0$.

The rationality of the FWHM of the antiresonance cavity, $\Delta\nu_{\mathrm{antires}}$, can be verified using the power reflection factor. The average of R_{max} and R_{min} is obtained through Eq. (2). Analogously, the FWHM of one of the reflection spectra is consistent with the result of Eq. (11).

The ratio between cavity bandwidth and FSR, and the finesse as a function of cavity reflectivity $R = r_1 r_2$, are shown in Figs. 3(a) and 3(b), respectively. The dash-dotted black line (approximate value) and solid red line (exact value) represent the calculations of the resonant cavity, and the short-dashed-dotted blue line (approximate value) and dashed green line (exact value) are the results for the antiresonant cavity. The insets correspond to the results with R being in the range 0–0.5. The black stars and black circles correspond to the experimental value obtained in our previous work [20,25]. This illustrates that the exact and approximate solutions of the cavity bandwidth (finesse) tend to be consistent with increasing R. Figure 3(a) [Fig. 3(b)] shows that the FWHM [finesse]

at resonance and antiresonance separately obtained by Eqs. (6) and (11) [Eqs. (7) and (12)] intersect at $R = 0$, which is a smooth transition. In contrast, the results obtained by approximate formulas are separated. In this paper, we put forward the exact expressions of the FWHM and finesse, which can successfully avoid the singularity problem in conventional expressions [24].

Moreover, using Eqs. (6) and (11), the cavity bandwidths of the resonant and antiresonant cavities both approach $R_{\mathrm{FS}}/2$ rather than infinity when $R \to 0$. In addition, the cavity bandwidths of the resonant and antiresonant cavities approach zero and FSR, respectively, with $R \to 1$. Similarly, the cavity finesse is equal to 2 rather than zero when the reflectivity $R = 0$. These results are important for the applications of an ultralow finesse cavity.

C. Symmetry characteristics of cavity-enhancement and cavity-inhibited factors

In this paper, the cavity-enhancement factor is analyzed by the above results. Owing to the Purcell effect [4], the spontaneous emission rate of the two-level atoms in a resonant cavity can be enhanced by $\eta_c = 3Q_c\lambda^3/4\pi^2V$ times compared with that in free space. $Q_c = \nu_0/\Delta\nu_c$ is the cavity quality factor, which is defined as the ratio of the atomic transition frequency to the cavity-mode linewidth of the resonant cavity. λ is the atomic transition wavelength and V represents the equivalent cavity mode volume. Therefore, the Purcell factor is proportional to the cavity quality factor, i.e., proportional to the cavity finesse. The resonant cavity enhances the spontaneous emission rate; conversely, the spontaneous emission rate is inhibited in an antiresonant cavity, which was first proven by Kleppner [29]. This shows that the inhibition factor is inversely proportional to the cavity finesse.

It is assumed that there is an atomic dipole in a concentric FP resonator, for which the radii of curvature of M_1 and M_2 are equal and their reflectivities $R_1 = R_2 = R$. In order to calculate the total power radiated by the dipole, we assume that the power is radiated in a spherical surface, which is divided into three parts: S_1, the part lying outside cavity mirror M_1; S_2, the part lying outside cavity mirror M_2; and S_{side}, the remainder of the sphere. S_1, S_2, and S_{side} subtend solid angles $\Delta\Omega_1$, $\Delta\Omega_2$, and $\Delta\Omega_{\mathrm{side}}$, respectively, where $\Delta\Omega_1 + \Delta\Omega_2 + \Delta\Omega_{\mathrm{side}} = 4\pi$, and the solid angle of the cavity can be expressed as $\Delta\Omega_c = \Delta\Omega_1 + \Delta\Omega_2$.

According to Ref. [30], the power passing through S_{side} is simply the total free space power P_{free} minus the power emitted into $\Delta\Omega_c$, and it can be expressed as

$$P_{\mathrm{side}} = \left(1 - \frac{3}{8\pi}\Delta\Omega_c\right)P_{\mathrm{free}}. \tag{16}$$

By calculating the power transmitted through S_1 and S_2, we find finally that

$$P_c = \frac{1 - R^2}{1 + R^2 - 2R\cos(\omega 2L/c)}P_{\mathrm{free}}, \tag{17}$$

where $R = r_1 r_2$ is the cavity reflectivity. This shows that the power radiated by the dipole to the cavity follows the Airy function line shape of the cavity.

Consequently, the total power emitted by the dipole can be simply written as the sum of the power radiated from the side and the power emitted from the cavity mirrors, and it is given by

$$P_{\mathrm{total}} = \left[1 + \left(\frac{1 - R^2}{1 + R^2 - 2R\cos(\omega 2L/c)} - 1\right)\frac{3}{8\pi}\Delta\Omega_c\right]P_{\mathrm{free}}. \tag{18}$$

According to Eq. (18), the power emitted into $\Delta\Omega_{\mathrm{side}}$ is fixed. As the phase of the reflected field is tuned, only the power emitted into $\Delta\Omega_c$ is changed. Therefore, the total power also follows the absorptive line shape of the cavity. In order to facilitate the analysis, we only study the change of the power radiated into the cavity with the phase shift.

Here, we define the ratio between the power radiated into the intracavity and into free space as $\alpha = P_c/P_{\mathrm{free}}$, which is a function of the phase shift. The maximum and the minimum values of α are $\alpha_{\max} = \frac{1+R}{1-R}$ and $\alpha_{\min} = \frac{1-R}{1+R}$, respectively, when the cavity is resonant and antiresonant.

Taking the resonant case as an example, the relationship between the cavity-enhancement factor and the cavity finesse under the limit of $R \to 1$ and 0 is analyzed separately.

(i) For $R \to 1$, $\alpha_{\max} = \frac{1+R}{1-R} \simeq \frac{2}{1-R}$, and $\mathcal{F}_r{}' = \frac{\pi\sqrt{R}}{1-R} \simeq \frac{\pi}{1-R}$. Therefore, $\alpha_{\max} = \frac{2\mathcal{F}_r{}'}{\pi}$.

(ii) For $R \to 0$, using the Taylor formula, $\frac{1}{1-R} = 1 + R + R^2 + \cdots$. Then, $\alpha_{\max} = \frac{1+R}{1-R} = \frac{2}{1-R} - 1 \simeq 1 + 2R$. According to Eq. (10), $\mathcal{F}_r{}'' \simeq 2 + \frac{8R}{\pi - 4R}$. Consequently, $\alpha_{\max} = 1 + \frac{\pi}{2\mathcal{F}_r{}''}(\mathcal{F}_r{}'' - 2)$. Moreover, $\mathcal{F}_r{}'' \to 2$ when $R \to 0$, which indicates that the cavity-enhancement factor approaches 1.

In summary, for a resonant cavity with $R \to 1$, the ratio can be reduced to $2\mathcal{F}_{\mathrm{r}}{}'/\pi$. For an antiresonant cavity, the ratio is $1/\frac{2\mathcal{F}_{\mathrm{r}}{}'}{\pi}$. This intuitively illustrates that the cavity-enhancement effect is obvious for a high-finesse cavity. In contrast, as for the ultralow-finesse cavity ($R \to 0$, close to mirrorless), α is close to 1 in both resonant and antiresonant cavities. This is reasonable because light can pass through the cavity almost unobstructed in an ultralow reflectivity cavity. Here, we give a general expression of the cavity-enhancement factor rather than one only confined to the condition of a high-finesse cavity. P_c/P_{free} as a function of phase shift is depicted in Fig. 4(a). To make the description more intuitive, Fig. 4(b) shows the change of ratio with phase shift in logarithmic scale. It is clear that, with decreasing reflectivity, the ratio gradually approaches 1, which means that the cavity-enhancement factor is 1 at $R = 0$. This is different from the classical expression of $2\mathcal{F}_r{}'/\pi$, which satisfies the condition of a high-reflectivity cavity and is inadequate for the high-loss case, since the cavity-enhancement factor should naturally reach 1 when the cavity-mirror reflectivity approaches zero. In addition, the enhancement factor of the resonant cavity and the inhibition factor of the antiresonant cavity are equal, i.e., the enhancement and the inhibition of intracavity light intensity by the resonant and antiresonant cavities are symmetrical, as depicted in Fig. 4(b).

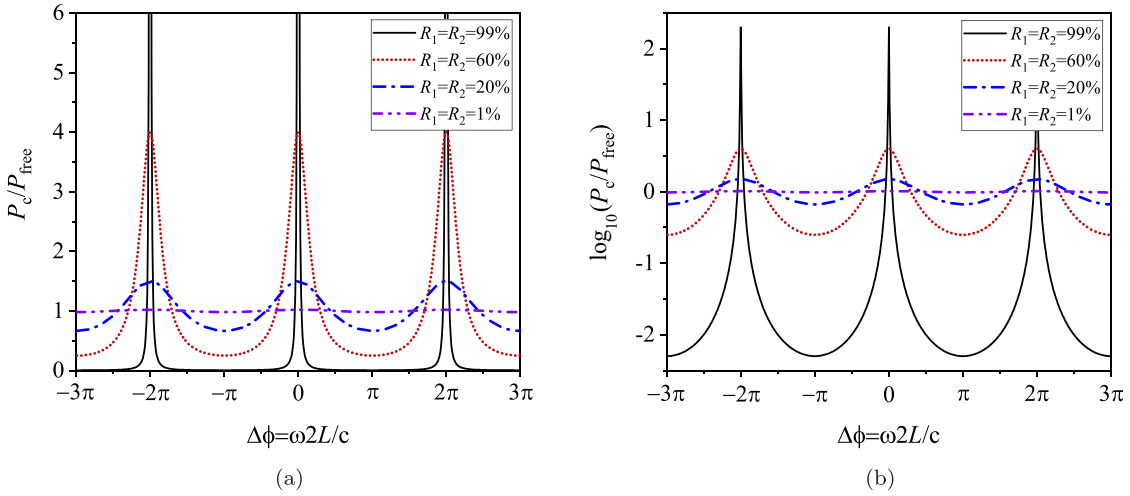

FIG. 4. Ratio of power emitted into a cavity to that into free space vs the phase shift in (a) linear and (b) logarithmic coordinates. The symmetry characteristics of the cavity-enhancement factor in the resonant cavity and cavity-inhibited factor in the antiresonant cavity are depicted. The solid black line, dashed red line, dashed-dotted blue line, and dashed-dotted purple line represent the results of $R_1 = R_2 = 99$, 60, 20, and 1%, respectively. As the reflectivity decreases, the ratio of P_c/P_{free} gradually approaches 1.

III. APPLICATION OF antiRESONANT ultraLOW-FINESSE FP CAVITY FOR REALIZATION OF the INHIBITED LASER

A. Inhibited laser

Although the enhancement factor is smaller than 1 for an antiresonant cavity, the stimulated emission can also be realized in an antiresonant, ultralow-finesse cavity [25]. As shown in Figs. 4(a) and 4(b), with decreasing reflectivity, the cavity-enhancement effect is gradually weakened at the resonant regime. Meanwhile, the cavity-inhibited effect in the antiresonant region is also gradually weakened. This is the key to realizing stimulated radiation in an antiresonant cavity.

According to Ref. [31], assuming that the cavity detuning is zero, the laser rate equation is expressed as

$$\frac{dn}{dt} = G - L' = \frac{N}{t_{\text{int}}}\sin^2(\sqrt{n+1}gt_{\text{int}}) - \Gamma_c n. \tag{19}$$

n is the intracavity photon number, and G and L' represent the gain and the loss, respectively. Gain greater than loss is a prerequisite for lasing. Here, we assume a cloud of atoms as the gain medium. N is the effective atomic number, t_{int} the interaction time between light and atom, g the atom-cavity coupling coefficient, and Γ_c the cavity dissipation rate.

If the cavity detuning is large enough that it is not negligible, the loss term should be rewritten as

$$L' = \Gamma_c n\frac{P_{\text{cmax}}}{P_c} = \Gamma_c n\left[1 + \frac{2R[1-\cos(\omega 2L/c)]}{(1-R)^2}\right]. \tag{20}$$

Here, we utilize Eq. (17), which reflects the change of intracavity loss with phase shift in the rate equation. The expression in square brackets is defined as the loss factor $\beta = \frac{P_{\text{cmax}}}{P_c} = 1 + \frac{2R[1-\cos(\omega 2L/c)]}{(1-R)^2}$. β as a function of phase shift is depicted in Fig. 5(a). Figure 5(b) shows the result under logarithmic coordinates. For a resonant cavity, the loss factor reaches a minimum $\beta_{\text{min}} = 1$, and the laser rate equation can be expressed by Eq. (19). However, regarding the antiresonant cavity, the loss factor is enhanced and reaches a maximum $\beta_{\text{max}} = 1 + \frac{4R}{(1-R)^2}$. According to Fig. 5(b), as $R \to 0$, the loss factor approaches 1 in both resonant and antiresonant regimes. Regarding $R \to 1$, the loss factor at resonance is $(\frac{2\mathcal{F}_r'}{\pi})^2$ times that at antiresonance. This also proves that the low-finesse resonator more easily realizes laser oscillation at the antiresonant region.

Moreover, the loss term can also be explained by the photon picture. τ_c is the average time of photons being stored in an optical resonator before they eventually escape through the output mirror. The loss term of Eq. (19) can be written as n/τ_c. If $R \to 0$, $\tau_c = L/c$, and then the loss term is nc/L. Regarding $R \to 1$, the average time is enhanced by $\frac{2\mathcal{F}_r'}{\pi}$ times to $\tau_c = \frac{2\mathcal{F}_r'}{\pi}\frac{L}{c}$, and the loss term becomes $\frac{n\Gamma_c}{2}$ utilizing $\mathcal{F}_r' = 2\pi\frac{R_{\text{FS}}}{\Gamma_c}$. In an antiresonant cavity, the average time is inhibited by $\frac{2\mathcal{F}_r'}{\pi}$ times; similarly, the loss term can be expressed as $\frac{n\Gamma_c}{2}(\frac{2\mathcal{F}_r'}{\pi})^2$. Hence, the ratio of the loss term at antiresonance to that at resonance is $(\frac{2\mathcal{F}_r'}{\pi})^2$, which verifies the above discussion.

In addition, this can be explained by examining Table I. $|E_{\text{in}}|^2$, P_c, and $|E_t|^2$ represent the light intensities incident on the first mirror, inside the cavity, and transmitted through the cavity, respectively. The initial light intensity is $|E_0|^2$. Table I shows the light intensity inside (or through) the FP cavity in resonant and antiresonant cavities separately.

Although most of the traditional lasers work in the resonant cavity, the use conditions of the photon-number equation

TABLE I. Light intensity inside or through the FP cavity. $|E_t|^2 = \frac{(1-R)^2}{1+R^2-2R\cos(\omega 2L/c)}|E_0|^2$; $P_c = \frac{1-R^2}{1+R^2-2R\cos(\omega 2L/c)}|E_0|^2$.

	$\lvert E_{\text{in}}\rvert^2$	P_c	$\lvert E_t\rvert^2$
Resonant	$\lvert E_0\rvert^2$	$\frac{1+R}{1-R}\lvert E_0\rvert^2$	$\lvert E_0\rvert^2$
Antiresonant	$\lvert E_0\rvert^2$	$\frac{1-R}{1+R}\lvert E_0\rvert^2$	$(\frac{1-R}{1+R})^2\lvert E_0\rvert^2$

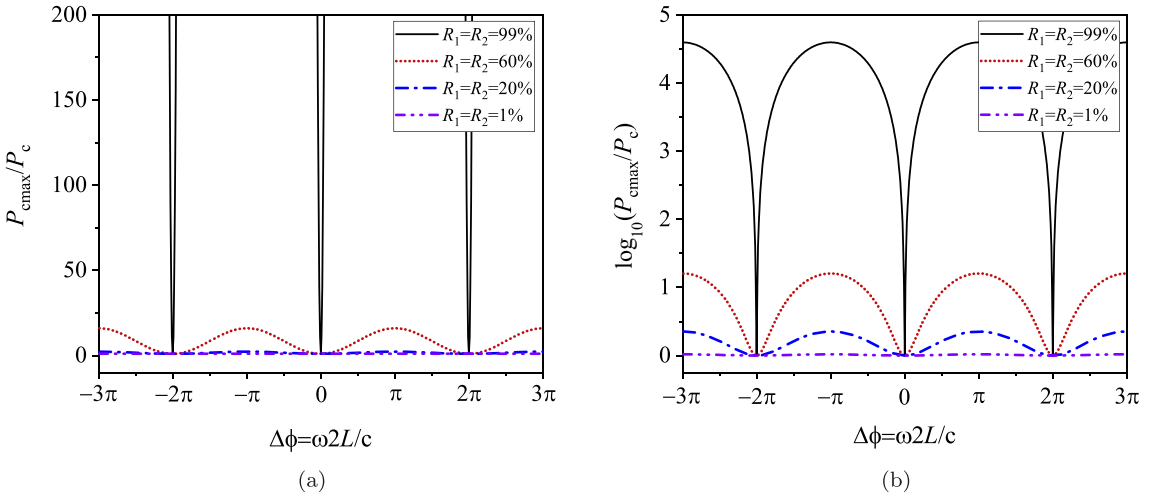

FIG. 5. Ratio of the maximal power emitted into the cavity to that into the cavity vs the phase shift in (a) linear and (b) logarithmic coordinates. The solid black line, red dots, dashed-dotted blue line, and dashed-dotted purple line represent the results of $R_1 = R_2 = 99$, 60, 20, and 1%, respectively. As the reflectivity decreases, the ratio of P_{cmax}/P_c gradually approaches 1.

describing this resonant laser are limited. Therefore, we give a universal expression that can derive the intracavity photon number at any cavity frequency. We demonstrate that the laser can also be realized in an antiresonant cavity.

B. Cavity-pulling coefficient

The cavity-pulling coefficients in the cases of spontaneous and stimulated radiations are analyzed, as shown in Table II. The results at R taking arbitrary values at resonant and antiresonant regimes are given separately. According to Heinzen and Feld [30], the level shift of an atom inside the optical resonator can be modified by the cavity. Furthermore, the shift in atomic radiation frequency is suppressed to zero with the spectral linewidth narrowed at the antiresonance regime, which is of great significance for precision measurement.

Here, we extend the results of frequency shift of radiation in Ref. [30] to the cavity-pulling coefficient, which is expressed as $C = \frac{d\omega}{d\omega_c}$, where ω and ω_c represent the radiation frequency and cavity-mode frequency, respectively. Letting R take an arbitrary value, the cavity-pulling coefficients of spontaneous radiation at resonant and antiresonant regimes are $\frac{2L}{c}\Gamma_0\frac{2R}{(1-R)^2}$ and $-\frac{2L}{c}\Gamma_0\frac{2R}{(1+R)^2}$, respectively. Γ_0 is the decay rate of the atomic dipole. Compared with the result in the resonant regime, the influence of the cavity-pulling effect on the radiation frequency in the antiresonant regime is suppressed $(\frac{1+R}{1-R})^2$ times, and is approximately $1+(\frac{2\mathcal{F}_{r'}}{\pi})^2$ when $R \to 1$.

Moreover, the cavity-pulling coefficients of stimulated radiation at resonant and antiresonant regimes are given. In a circumstance of stimulated radiation, the focus is always on the cavity-pulling coefficient at the resonant cavity, where lasing is traditionally achieved. However, the cavity-pulling coefficient of an inhibited laser is also critical. The cavity-pulling coefficient of a laser working in the resonant cavity is $\frac{\Gamma_0}{\Gamma_0+\Gamma_c}$. If the laser works in the good-cavity limit, where $\Gamma_0 \gg \Gamma_c$, $C \approx 1$. In contrast, $C \ll 1$ for AOC lasers [13–22] working in the bad-cavity limit. Therefore, the sensitivity of AOC lasers to cavity-length thermal noise is greatly reduced, and it is characterized by the suppressed cavity-pulling effect. Analogous to the spontaneous result, compared with a resonant AOC laser, the influence of cavity-length noise on the frequency of an inhibited laser is further suppressed by a factor of $(\frac{1+R}{1-R})^2$ times, as shown in Table II.

This indicates that the influence of cavity-length thermal noise on the frequency of an inhibited laser is smaller compared to a traditional resonant laser. However, it should be noted that, for the inhibited laser, if we keep the cavity dissipation rate constant, the higher the cavity finesse (or cavity-mirror reflectivity), the stronger the suppression of cavity-length noise, and the lower output power. Hence, to balance the output power and suppression of the cavity-pulling effect of an inhibited laser, we must set the cavity finesse to an appropriate value. Nevertheless, the development of an inhibited laser is of great significance for the field of precision measurement.

TABLE II. Cavity-pulling coefficients in the optical domain. $\frac{2L}{c} = \frac{2\pi}{\mathcal{F}_r}\frac{1}{\Gamma_c}$; $R \to 1$, $\mathcal{F}_r = \mathcal{F}_{r'} = \frac{\pi\sqrt{R}}{1-R}$ [Eq. (9)].

	Spontaneous		Stimulated	
	R (arbitrary)	$R \to 1$	R (arbitrary)	$R \to 1$
Resonant	$\frac{2L}{c}\Gamma_0\frac{2R}{(1-R)^2}$	$\frac{2\mathcal{F}_{r'}}{\pi}\frac{\Gamma_0}{\Gamma_c}$	$\frac{\Gamma_0}{\Gamma_c}$	
Antiresonant	$-\frac{2L}{c}\Gamma_0\frac{2R}{(1+R)^2}$	$-\frac{2\mathcal{F}_{r'}}{\pi}\frac{1}{1+(2\mathcal{F}_{r'}/\pi)^2}\frac{\Gamma_0}{\Gamma_c}$	$(\frac{1-R}{1+R})^2\frac{\Gamma_0}{\Gamma_c}$	$-\frac{1}{1+(2\mathcal{F}_{r'}/\pi)^2}\frac{\Gamma_0}{\Gamma_c}$

IV. CONCLUSIONS

Because the Airy function of a low-finesse FP cavity is flat compared with the high-finesse cavity, the effect of cavity-length thermal noise on the laser frequency can be greatly suppressed. The low-finesse cavity is preferred for the realization of AOCs and inhibited lasers, which is significant for quantum metrology and may lead to new research in the laser physics and cavity quantum electrodynamics fields. Therefore, it is highly necessary to derive the exact expressions describing the cavity characteristics.

In this paper, we present the exact expressions describing characteristics of a FP cavity, such as the cavity finesse and FWHM, as well as the cavity-enhancement and -inhibited factors. In particular, the exact expressions of finesse and FWHM expand the result at the traditional high-reflectivity approximation to the arbitrary reflectivity case, and solve the singularity problem in traditional expressions. This proves that the cavity finesse is equal to 2 rather than zero at $R = 0$. Moreover, the symmetry characteristics of cavity-enhancement and -inhibited factors are analyzed, which clearly show the impact of the cavity on light power. Furthermore, the characteristics of the antiresonant cavity, where the cavity frequency is between two adjacent cavity modes, are also demonstrated. The antiresonant cavity proposed in this paper is of great significance for realizing an inhibited laser, which would be relevant for quantum precision metrology and have new applications in fundamental and applied science, such as in the study of fundamental constant variations and relativistic geodesy.

ACKNOWLEDGMENTS

This research was funded by the National Natural Science Foundation of China (Grant No. 91436210), China Postdoctoral Science Foundation (Grant No. BX2021020), and Wenzhou Major Science and Technology Innovation Key Project (Grant No. ZG2020046).

[1] R. W. P. Drever, J. L. Hall, F. V. Kowalski, J. Hough, G. M. Ford, A. J. Munley, and H. Ward, Laser phase and frequency stabilization using an optical resonator, Appl. Phys. B **31**, 97 (1983).

[2] R. V. Pound, Electronic frequency stabilization of microwave oscillators, Rev. Sci. Instrum. **17**, 490 (1946).

[3] D. G. Matei, T. Legero, S. Häfner, C. Grebing, R. Weyrich, W. Zhang, L. Sonderhouse, J. M. Robinson, J. Ye, F. Riehle, and U. Sterr, 1.5μm Lasers with Sub-10 mHz Linewidth, Phys. Rev. Lett. **118**, 263202 (2017).

[4] E. M. Purcell, Spontaneous emission probabilities at radio frequencies, Phys. Rev. **69**, 37 (1946).

[5] P. Goy, J. M. Raimond, M. Gross, and S. Haroche, Observation of Cavity-Enhanced Single-Atom Spontaneous Emission, Phys. Rev. Lett. **50**, 1903 (1983).

[6] D. J. Heinzen, J. Childs, C. Monroe, J. E. Thomas, and M. S. Feld, Enhanced and Inhibited Visible Spontaneous Emission by Atoms in a Confocal Resonator, Phys. Rev. Lett. **58**, 1320 (1987).

[7] F. D. Martini, G. Innocenti, G. R. Jacobovitz, and P. Mataloni, Anomalous Spontaneous Emission Time in a Microscopic Optical Cavity, Phys. Rev. Lett. **59**, 2955 (1987).

[8] W. R. Bennett, Hole burning effects in a He-Ne optical maser, Phys. Rev. **126**, 580 (1962).

[9] T. J. Kane and R. L. Byer, Monolithic, unidirectional single-mode Nd:YAG ring laser, Opt. Lett. **10**, 65 (1985).

[10] D. J. Thompson and R. E. Scholten, Narrow linewidth tunable external cavity diode laser using wide bandwidth filter, Rev. Sci. Instrum. **83**, 023107 (2012).

[11] C. Monroe, D. M. Meekhof, B. King, W. M. Itano, and D. Wineland, Demonstration of a Fundamental Quantum Logic Gate, Phys. Rev. Lett. **75**, 4714 (1995).

[12] T. Kessler, C. Hagemann, C. Grebing, T. Legero, U. Sterr, F. Riehle, M. J. Martin, L. Chen, and J. Ye, A sub-40-mHz-linewidth laser based on a silicon single-crystal optical cavity, Nature Photon **6**, 687 (2012).

[13] J. Chen, Active optical clock, Chin. Sci. Bull. **54**, 348 (2009).

[14] D. Meiser, J. Ye, D. R. Carlson, and M. J. Holland, Prospects for a Millihertz-Linewidth Laser, Phys. Rev. Lett. **102**, 163601 (2009).

[15] J. G. Bohnet, Z. Chen, J. M. Weiner, D. Meiser, M. J. Holland, and J. K. Thompson, A steady-state superradiant laser with less than one intracavity photon, Nature (London) **484**, 78 (2012).

[16] G. A. Kazakov and T. Schumm, Active optical frequency standard using sequential coupling of atomic ensembles, Phys. Rev. A **87**, 013821 (2013).

[17] W. Zhuang and J. Chen, Active faraday optical frequency standard, Opt. Lett. **39**, 6339 (2014).

[18] M. A. Norcia, J. R. K. Cline, J. A. Muniz, J. M. Robinson, R. B. Hutson, A. Goban, G. E. Marti, J. Ye, and J. K. Thompson, Frequency Measurements of Superradiance from the Strontium Clock Transition, Phys. Rev. X **8**, 021036 (2018).

[19] T. Laske, H. Winter, and A. Hemmerich, Pulse Delay Time Statistics in a Superradiant Laser with Calcium Atoms, Phys. Rev. Lett. **123**, 103601 (2019).

[20] T. Shi, D. Pan, and J. Chen, Realization of phase locking in good-bad-cavity active optical clock, Opt. Express **27**, 22040 (2019).

[21] S. A. Schäffer, M. Tang, M. R. Henriksen, A. A. Jørgensen, B. T. R. Christensen, and J. W. Thomsen, Lasing on a narrow transition in a cold thermal strontium ensemble, Phys. Rev. A **101**, 013819 (2020).

[22] H. Liu, S. B. Jäger, X. Yu, S. Touzard, A. Shankar, M. J. Holland, and T. L. Nicholson, Rugged mHz-Linewidth Superradiant Laser Driven by a Hot Atomic Beam, Phys. Rev. Lett. **125**, 253602 (2020).

[23] D. Pan, T. Shi, and J. Chen, Dual-wavelength good-bad-cavity laser system for cavity-stabilized active optical clock, IEEE Tans. Ultrason. Ferroelectr. Freq. Control **65**, 1958 (2018).

[24] N. Ismail, C. C. Kores, D. Geskus, and M. Pollnau, Fabry-Pérot resonator: Spectral line shapes, generic and related airy distributions, linewidths, finesses, and performance at low

or frequency-dependent reflectivity, Opt. Express **24**, 16366 (2016).

[25] T. Shi, D. Pan, and J. Chen, An inhibited laser, Commun. Phys. **5**, 208 (2022).

[26] J. M. Robinson, E. Oelker, W. R. Milner, W. Zhang, T. Legero, D. G. Matei, F. Riehle, U. Sterr, and J. Ye, Crystalline optical cavity at 4 K with thermal-noise-limited instability and ultralow drift, Optica **6**, 240 (2019).

[27] A. E. Siegman, *Lasers* (University Science, Mill Valley, CA, 1986).

[28] F. Riehle, *Frequency Standards: Basics and Applications* (Wiley, New York, 2004).

[29] D. Kleppner, Inhibited Spontaneous Emission, Phys. Rev. Lett. **47**, 233 (1981).

[30] D. J. Heinzen and M. S. Feld, Vacuum Radiative Level Shift and Spontaneous-Emission Linewidth of an Atom in an Optical Resonator, Phys. Rev. Lett. **59**, 2623 (1987).

[31] C. M. Fang-Yen, Multiple thresholds and many-atom dynamics in the cavity QED microlaser, Ph.D. thesis, Massachusetts Institute of Technology, 2002.